Analysis and control of epidemics in temporal networks with self-excitement and behavioral changes

Analysis and control of epidemics in temporal networks with self-excitement and behavioral changes

Lorenzo Zino[a,c,b], Alessandro Rizzo[d,e,*], Maurizio Porfiri[a,f,*]

[a] *Department of Mechanical and Aerospace Engineering, New York University Tandon School of Engineering, Brooklyn NY 11201, USA*
[b] *Faculty of Science and Engineering, University of Groningen, 9747 AG Groningen, The Netherlands*
[c] *"G.L. Lagrange" Department of Mathematics, Politecnico di Torino, 10129 Torino, Italy*
[d] *Department of Electronics and Telecommunications, Politecnico di Torino, 10129 Torino, Italy*
[e] *Office of Innovation, New York University Tandon School of Engineering, Brooklyn NY 11201, USA*
[f] *Department of Biomedical Engineering, New York University Tandon School of Engineering, Brooklyn NY 11201, USA*

Abstract

The complexity of interaction patterns among individuals in social systems plays a fundamental role on the inception and spreading of epidemic outbreaks. Empirical evidence has shown that the network of social interactions may co-evolve with the spread of the disease at comparable time-scales. Time-varying features have also been documented in the study of the propensity of individuals toward social activity, leading to the emergence of burstiness and temporal clustering. These temporal network dynamics are not independent of the disease evolution, whereby infected individuals could experience changes in their tendency to form connections, spontaneously or due to exogenous control policies. Neglecting these phenomena in modeling epidemics could lead to dangerous mispredictions of an outbreak and ineffective control interventions. In this paper, we propose a mathematically tractable modeling framework that relies on a limited number of parameters and encapsulates all these instances of complex phenomena through the lens of activity driven networks. Hawkes processes, Markov chains,

*Corresponding authors
Email addresses: lorenzo.zino@rug.nl (Lorenzo Zino), alessandro.rizzo@polito.it (Alessandro Rizzo), mporfiri@nyu.edu (Maurizio Porfiri)

and stability theory are leveraged to assist in the analysis of the framework and the formulation of theory-based control interventions. Our mathematical findings confirm the intuition that bursty activity patterns, typical of humans, facilitate epidemic spreading, while behavioral changes aiming at individual isolation could accelerate the eradication of epidemics. The proposed tools are demonstrated on a real-world case of influenza spreading in Italy. Overall, this work contributes new insight into the theory of temporal networks, laying the foundations for analysis and control of spreading processes on networks with complex interaction patterns.

Keywords: activity driven network, epidemic threshold, Hawkes process, self-excitement, time-varying

1. Introduction

Our increased capability of collecting and analyzing large datasets has promoted an unprecedented understanding about patterns and formation mechanisms of social interactions in human communities. Many empirical studies have revealed that networks of social interactions continuously evolve in time, where each individual dynamically generates and modifies his/her connections with others [1, 2, 3]. In real applications, this network evolution develops on a time-scale that is comparable with epidemic processes running on its fabric [4], thereby limiting the use of time-scale separation approaches [5]. As a result, in most practical settings, neither one can assume that contacts are constant in time to work with a static network [6], nor one can invoke the fast-switching limit to deal with an annealed network [7]. Just as one cannot dismiss time variations for the network, one should not neglect time-varying features in the individuals' propensity to generate connections, which are responsible for the emergence of bursty patterns [8] and temporal clustering of interactions [9, 10, 11, 12].

The link generation dynamics and individual propensity to create links may be triggered by self-excitement mechanisms [13, 14, 15]. Many forms of social

interactions are driven by gratification dynamics that yield self-sustaining mechanisms, whereby the more one individual is socially active, the more he/she is motivated to increase his/her propensity to connect with others. Hence, self-excitement contributes to the emergence of heterogeneous temporal patterns of social activity, with burstiness and temporal clustering [14, 16, 17]. The state of health of individuals has also an important role in shaping their propensity to generate connections. For instance, infected individuals may spontaneously tend to reduce their activity as a consequence of the disease [18, 19]. Such an activity reduction can also be enforced by administrations that could seek to establish effective countermeasures, including awareness campaigns, quarantine, and hospitalization [20, 21].

Motivated by this evidence, herein we investigate the combined effect of these complex phenomena on both the formation of the network of contacts and the concurrent epidemic spreading. Our work seeks to understand the role of these phenomena on the emergence of epidemic outbreaks and, possibly, inform the design of control policies that can be adopted by public health authorities to achieve fast eradication of epidemic diseases. We model the temporal network of interactions within the framework of activity driven networks (ADNs), which has emerged as a powerful lens to study time-varying networks of interactions [4]. The main advantage of this modeling choice lies in its simplicity, whereby the temporal nature of the network could be in principle consolidated into a single constant parameter associated with each individual, the so-called activity. The activity represents the propensity of an individual to generate temporal connections with others, and can easily be inferred from empirical data [4, 22, 23, 24]. Once the distribution of the activities is known, the pattern of connections is generated following a probabilistic mechanism, implemented as the system evolves in time.

In the recent literature, the ADN paradigm has been extended along many directions to include several real-world features that favor the representation and the rigorous analysis of important phenomena. These real-world features comprise epidemic evolution on continuous time-scales [25, 26], heterogeneous

propensity of nodes to receive connections [27, 28], nontrivial community structures [29, 30], recurrent connections [31, 32], and high-order relationships [33]. The original ADN and its extensions are often amenable to analytical tractability, thereby enabling the scientific community to unveil the role of temporal patterns in epidemiology [24, 26], opinion dynamics [34], diffusion of innovation [35] and rumors [36], and percolation problems [37].

Despite these major advancements, only few attempts have been made to encapsulate temporal features of human social behavior. Among those, we should mention the inclusion of memory in the link generation mechanism [38, 39], which has a nontrivial role on the spread of epidemics. Based on numerical simulations and long-run approximations, memory could favor epidemic spreading in the absence of immunization after recovery, while the opposite effect could be triggered in the presence of immunization mechanisms [38]. Another important step in this direction has been undertaken by considering behavioral changes associated with health status or awareness of epidemic spreading [24, 40, 41]. Finally, recent efforts have examined burstiness in human behavior through the cogent modification of the inter-event distribution of connection patterns [42, 43]. However, including memory or burstiness strains the Markov property of the model, thereby hindering analytical tractability.

Here, we propose a mathematical framework for epidemic spreading on ADNs that encapsulates self-excitement and behavioral changes in the individual dynamics. Toward this aim, the time-homogeneous activation mechanisms of the original ADNs [4, 25] is replaced with Hawkes processes [44]. Hawkes processes are a family of stochastic processes, which have often been used in seismology [45]. Their main advantages are that they rely on a small number of parameters, they satisfy the Markov property, and they exhibit an emergent behavior with burstiness and temporal clustering. Hence, the use of these processes preserves the Markov property and the simple formulation of ADNs, thereby favoring rigorous analysis of the system along with fast Monte Carlo simulations based on the Gillespie algorithm [46]. In the first implementation of this model, proposed in [47], the effect of self-excitement on the asymptotic

distribution of the activities and on the epidemic threshold of a susceptible–infected–susceptible (SIS) epidemic model have been studied, demonstrating that self-excitement promotes the inception of epidemic diseases by decreasing the epidemic threshold.

We build on [47] to establish a mathematical framework for epidemic models with self-excitement mechanisms and activity reduction of infected nodes. An important objective is to provide a viable method to identify model parameters from epidemic data. In fact, classical parameter estimation algorithms for Hawkes processes requires to keep track of all the individuals' social interactions [48, 49], which is not reasonable in real-world scenarios. Inspired by [50], we develop and demonstrate an algorithm to identify model parameters from epidemic data sampled at the population level and we test it against available data on the 2018–2019 seasonal influenza in Italy. Within this framework, an analytical study of the SIS epidemic model is performed. This study unveils the interplay between self-excitement and activity reduction. In the absence of activity reduction, self-excitement favors the inception and evolution of the epidemics; while in the absence of self-excitement, activity reduction has the opposite effect. When both phenomena are taken into consideration, two regions of the parameter space are analytically characterized: one where the effect of self-excitement overcomes activity reduction, and the other where the opposite occurs. We conclude the paper by studying the effectiveness of control strategies construed upon these features. Numerical simulations are provided to corroborate our findings.

The main theoretical contributions of this work are: *i*) the formalization of a general epidemic model on ADNs that include self-excitement and activity reduction due to the health state of infected nodes; *ii*) the development of a parameter identification algorithm for the parameters introduced with the self-excitement mechanism using epidemic data at the population level; *iii*) the rigorous analysis of the SIS epidemic model within the proposed modeling framework, with explicit computation of its epidemic threshold; and *iv*) the discussion of control techniques based on the activity reduction of infected

individuals, with an analytical assessment of the optimal value of the activity reduction. Beside these theoretical contributions, the paper also presents some experimental contributions. Specifically, *i*) the viability of the parameter identification algorithm is tested against available data on the 2018–2019 seasonal influenza in Italy; *ii*) the epidemic threshold for the SIS epidemic model is numerically estimated via Monte Carlo simulations, validating the analytical predictions; and *iii*) the theoretically-determined optimal value of the activity reduction is numerically verified through Monte Carlo simulations on the case study of the 2018–2019 seasonal influenza in Italy.

This paper completes and extends our preliminary work in [51] along several directions. First, the epidemic model is generalized and an algorithm to estimate the model parameters from empirical epidemic data at the population level is proposed. Second, a compelling array of mathematical proofs to support all of the main results is provided. Third, the discussion on the superimposition of self-excitement and activity reduction of infected individuals is extended by examining control techniques based on hospitalization and quarantine. Finally, a deeper review of related literature is presented to offer more context to the problem and help framing its mathematical objectives.

The rest of the paper is organized as follows. In Section 2, we present some mathematical preliminaries. In Section 3, we illustrate the network epidemic model. Section 4 is devoted to the description of the parameter identification algorithm. Section 5 is devoted to the analysis of the SIS model. In Section 6, we discuss the application of our approach to design control interventions that use the activity reduction of infected individuals. Section 7 summarizes our key findings and identifies areas of future research.

2. Mathematical preliminaries

2.1. Notation

We gather here the notation used throughout this paper. We denote by $\mathbb{R}_{\geq 0}$ the set of nonnegavive real numbers, by $\mathbb{R}_{>0}$ the set of strictly positive real

numbers, by $\mathbb{N}$ the set of nonnegative integer numbers, and by $\mathbb{Z}^+$ the set of strictly positive integer numbers. $\mathbb{P}[\cdot]$ denotes the probability of an event and $\mathbb{E}[\cdot]$ the expected value of a random variable.

2.2. Poisson point processes and Hawkes processes

The occurrences of stochastic events are often modeled through Poisson point processes [52]. A point process can be conveniently represented by means of its counting process $N(t) \in \mathbb{N}$, where $N(t)$ is the number of events registered up to time t. Poisson point processes are formally defined as follows.

Definition 1. *Let $a(t)$ be a locally integrable nonnegative function called intensity. Then, a Poisson point process verifies $N(0) = 0$, and, for any $\Delta t \in \mathbb{R}_{>0}$,*

$$\mathbb{P}[N(t + \Delta t) - N(t) = 1] = \int_t^{t+\Delta t} a(s)ds + o(\Delta t). \tag{1}$$

In the literature, it is often assumed that the intensity is constant, that is, $a(t) = a \in \mathbb{R}_{>0}$ for any $t \in \mathbb{R}_{\geq 0}$ [4, 25]. Under this assumption, Poisson processes are called homogeneous and (1) reduces to

$$\mathbb{P}[N(t + \Delta t) - N(t) = 1] = a\Delta t + o(\Delta t). \tag{2}$$

The choice of using (2) to model the timing of events in social interactions brings key simplifications that can lead to detailed analytical insight. However, such a choice neglects the well-known phenomena of burstiness and temporal clustering [8, 9, 10, 11, 12]. To include these features, we adopt Hawkes processes [44], where the intensity $a(t)$ varies in time according due to self-excitement.

Definition 2. *A Hawkes process is a Poisson point process with counting process $N(t)$, whose intensity $a(t)$ evolves according to the stochastic differential equation [53]*

$$da(t) = \gamma\left(\hat{a} - a(t)\right)dt + JdN(t), \tag{3}$$

where $J \in \mathbb{R}_{\geq 0}$, $\hat{a} \in \mathbb{R}_{>0}$, and $\gamma \in \mathbb{R}_{>0}$ are three constants and $N(t)$ is related to $a(t)$ through (1).

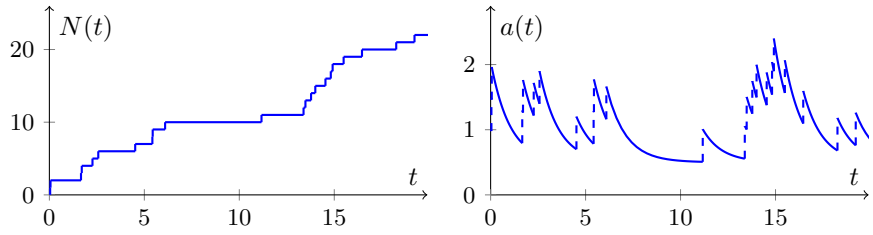

(a) Sample path (b) Intensity

Figure 1: Sample path (a) and intensity (b) of a Hawkes process with $\hat{a} = 0.75$, $J = 0.5$, $\gamma = 2$, and initial intensity $a(0) = 1$. The dashed vertical lines in (b) correspond to the increase of the intensity after each event. The onset of burstiness can be easily observed from the plot of intensity, whereby events tend to cluster in correspondence of the intensity peaks. These graphs are generated by numerically integrating (1) and (3), as shown in [54].

Since the evolution of $N(t)$ and $a(t)$ depends only on the current state of the system (counting process and intensity), Hawkes processes satisfy the Markov property, as explicitly proved in [44, 49]. The three parameters of Hawkes processes regulate their dynamics as follows:

i) the background intensity $\hat{a}$ represents the intensity in the absence of self-excitement, such that $a(t) \to \hat{a}$ as $t \to \infty$ for $J = 0$ in (3);

ii) the jump J quantifies the increase of the intensity after each event; and

iii) the forgetting rate γ determines the rate at which the intensity recovers its background value in (3).

From the numerical simulation of a Hawkes process, illustrated in Fig. 1, one can appreciate the temporal clustering of the events, along with the emergence of burstiness in the intensity. The presence of these phenomena constitutes promising evidence to employ Hawkes processes for the study of social interactions within the ADN paradigm. Alternative strategies to include burstiness into network models have been proposed in [55, 56]. However, these models rely on non-Poisson processes, that challenge their analytical treatment, as they do not share the Markov property.

We conclude this section by recalling a result on the asymptotic behavior of Hawkes process, which is used in the following of the paper; its proof can be found in [49].

Lemma 1. *Let $(N(t), a(t))$ be a Hawkes process with $J < \gamma$. Then, the first two moments of $a(t)$ are*

$$\mathbb{E}[a(t)] = \frac{\hat{a}}{1 - J/\gamma} + \left(a(0) - \frac{\hat{a}}{1 - J/\gamma} \right) e^{-(\gamma - J)t}, \tag{4a}$$

and

$$\begin{aligned} \mathbb{E}[a^2(t)] \quad = \quad & \frac{\hat{a}^2}{(1 - J/\gamma)^2} + \frac{J^2 \hat{a}}{2\gamma (1 - J/\gamma)^2} \\ & + \left[\left(a(0) - \frac{\hat{a}}{1 - J/\gamma} \right)^2 - \frac{J^2 \left(2a(0) - \frac{\hat{a}}{1 - J/\gamma} \right)}{2\gamma (1 - J/\gamma)} \right] e^{-2(\gamma - J)t} \\ & + \left[\frac{2 \left(a(0) - \frac{\hat{a}}{1 - J/\gamma} \right) \hat{a}}{1 - J/\gamma} + \frac{J^2 \left(a(0) - \frac{\hat{a}}{1 - J/\gamma} \right)}{\gamma (1 - J/\gamma)} \right] e^{-(\gamma - J)t}. \end{aligned} \tag{4b}$$

In the asymptotic limit of $t \to \infty$, we establish

$$\lim_{t \to \infty} \mathbb{E}[a(t)] = \frac{\hat{a}}{1 - J/\gamma}, \tag{5a}$$

and

$$\lim_{t \to \infty} \mathbb{E}[a^2(t)] = \frac{\hat{a}^2 + \frac{J^2 \hat{a}}{2\gamma}}{(1 - J/\gamma)^2}. \tag{5b}$$

Remark 1. *From Lemma 1, we comment that the behavior of the first two moments of the intensity exhibits the following characteristics:*

- *the increase in the asymptotic average intensity in* (5a) *is controlled by the ratio $J/\gamma \in [0, 1)$: when the ratio is equal to 0, the average intensity coincides with the background one; while it grows as the ratio tends to 1;*
- *the asymptotic variability of the intensity, measured by the coefficient of variation, that is, $c_v(t) = \sqrt{\mathbb{E}[a^2(t)]/\mathbb{E}[a(t)]^2}$, is regulated by the ratio*

$J^2/\gamma \in \mathbb{R}_{\geq 0}$*: the larger is the ratio, the broader is the asymptotic distribution of the intensity;*

- *the exponential rate of convergence to the asymptotic quantities in* (5a) *and* (5b) *is determined by the difference* $\gamma - J \in \mathbb{R}_{>0}$*, as shown in* (4a) *and* (4b)*. Slow convergence occurs if either i)* J *and* γ *are both close to* 0 *(such that self-excitement is negligible), or ii)* J *and* γ *are large, but very close to each other (that is, the system is close to the phase transition at* $J = \gamma$*). Hence, if self-excitement is nonnegligible and the system is bounded away from the phase transition (that is,* $J < \gamma$*), exponential convergence is always attained.*

3. The modeling framework

3.1. The network model

The population is modeled as a time-varying graph $\mathcal{G} = (\mathcal{V}, \mathcal{E}(t))$, where each individual is associated with a node in the set $\mathcal{V} = \{1, \dots, n\}$, while time-varying undirected links are collected in the set $\mathcal{E}(t)$. The time-varying adjacency matrix of the graph is defined as $A(t) \in \{0,1\}^{n \times n}$ such that $A_{ij}(t) = 1 \iff (i,j) \in \mathcal{E}(t)$ and $A_{ij}(t) = 0$, otherwise. Since the graph is undirected, matrix $A(t)$ is symmetric for any $t \in \mathbb{R}_{\geq 0}$. The network dynamics follows a continuous-time ADN [25, 26], where nodes' activations are regulated by Hawkes processes $(N_v(t), a_v(t))$, for each $v \in \mathcal{V}$. When a node v activates, it generates a temporal link, independent of the others. In order to avoid the introduction of an excessively large number of parameters, we assume that all of the Hawkes processes have the same jump $J \in \mathbb{R}_{\geq 0}$ and the same forgetting rate $\gamma \in \mathbb{R}_{>0}$, while background and initial activities can differ from a node to the others. Therefore, the heterogeneity of the system is modeled via the background activity $\hat{a}_v \in \mathbb{R}_{>0}$, which, in general, can differ from a node to the other, so that we refer to $\hat{a} \in \mathbb{R}^n_{>0}$ as a distribution on the nodes of the network. We refer to this model as the ADN+HP (activity driven network plus Hawkes processes), and its generation algorithm is summarized in the following steps:

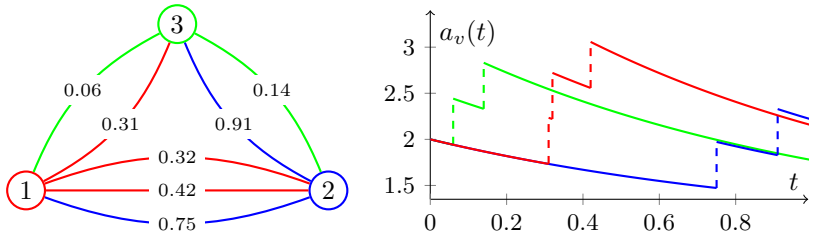

(a) Links and time-stamps (b) Nodes' activity

Figure 2: Simulation of an ADN+HP with $n = 3$ nodes for $T = 1$. In (a), each link is plotted along with the time-stamp of its occurrence. The color of the link identifies the node that has generated it. In (b), it is represented the temporal evolution of nodes' activities. Jump, forgetting rate, and background intensity are $J = 0.5$, $\gamma = 1$, and $\hat{a}_v = 1$, respectively. In addition, we set the initial condition $a_v(0) = 2$ for all the nodes.

1. at time $t = 0$, for each node $v \in \mathcal{V}$, we initialize an independent Hawkes process $(N_v(t), a_v(t))$ with initial intensity $a_v(0) \in \mathbb{R}_{\geq 0}$, and we set $\mathcal{E}(0) = \emptyset$;

2. if the Hawkes process associated with node v has a jump at time $t \in \mathbb{R}_{>0}$, then the corresponding node is said to be active and generates an undirected connection with a node in $w \in \mathcal{V}$, chosen uniformly at random. Such a link $\{v, w\}$ is added to $\mathcal{E}(t)$; and

3. the link is instantaneously removed from the link set, and the algorithm resumes from step 2.

Since all the Hawkes processes are independent of one another, one can conclude that at most one node is active at each time $t \in \mathbb{R}_{\geq 0}$ almost surely [52]. Therefore, for any $t \in \mathbb{R}_{\geq 0}$, the following properties hold almost surely: either 0 or 1 links belong to the link set $\mathcal{E}(t)$, and the adjacency matrix $A(t)$ has either 0 or 2 nonzero entries. Figure 2 presents a realization of an ADN+HP that illustrates the temporal evolution of the nodes' activities.

When considering the temporal evolution of an ADN+HP over a time-window of duration $T \in \mathbb{R}_{>0}$ from time t to time $t + T$, one can observe

from (1) that the expected number of times node $i \in \mathcal{V}$ is activated is equal to $\int_t^{t+T} \mathbb{E}[a(s)]ds$. Utilizing Lemma 1, we conclude that, in the asymptotic limit of $t \to \infty$, node i is activated on average $a_i T/(1 - J/\gamma)$ times, leading to an average of $a_i T/(1 - J/\gamma)(n - 1)$ interactions with any other node. Further details on the characteristics of the time-varying network can be found in [47].

In this paper, we make the following assumption, which allows us to apply Lemma 1.

Assumption 1. *All Hawkes processes have $J < \gamma$.*

Assumption 1 naturally arises in real-world applications. In fact, the expected value of the activity of a Hawkes process with $J \geq \gamma$ grows unbounded and blows up as time grows [49], which cannot describe real systems. Hence, we assume $J < \gamma$ for Hawkes processes associated with the frequency of human interactions.

Remark 2. *In the limit case of $J = 0$ and $a(0) = \hat{a}$, the ADN+HP model reduces to the standard continuous-time ADN model [25]. Therefore, the ADN+HP model encompasses and generalizes the original ADNs.*

We conclude this section with a claim on the effect of self-excitement on the activity distribution, which will be used later in the analysis of epidemics on ADNs+HP. Defining the moments of the activity distribution as

$$\langle a^i(t) \rangle := \frac{1}{n} \sum_{v \in \mathcal{V}} a_v^i(t), \quad i \in \mathbb{Z}, \tag{6}$$

the following claim can be stated; details can be found in [47].

Lemma 2. *For $n \to \infty$, under Assumption 1, the first two moments of the activity distribution converge exponentially almost surely to*

$$\lim_{t \to \infty} \langle a(t) \rangle = \frac{\langle \hat{a} \rangle}{1 - J/\gamma}, \tag{7a}$$

and

$$\lim_{t \to \infty} \langle a^2(t) \rangle = \frac{\langle \hat{a}^2 \rangle + \dfrac{J^2}{2\gamma} \langle \hat{a} \rangle}{(1 - J/\gamma)^2}, \tag{7b}$$

where the moments of the background intensity are defined similar to (6)*, averaging the values of the corresponding powers of background activities over the network nodes.*

3.2. Epidemics on ADN+HP

Here, we propose a general framework to describe an epidemic outbreak on an ADN+HP that incorporates activity reduction of infected individuals. Then, in Section 5, we examine the behavior of a specific incarnation of such an epidemic model, the SIS model, in the thermodynamic limit of $n \to \infty$.

According to [25], with each individual $v \in \mathcal{V}$ we associate a discrete state $Y_v(t)$, chosen from a finite set of health states. In the simplest case, we have $Y_v(t) \in \{S, I\}$, where

$$Y_v(t) = \begin{cases} S & \text{if } v \text{ is susceptible to the disease at time } t \\ I & \text{if } v \text{ is infected at time } t. \end{cases} \tag{8}$$

Several variants of this model can be introduced by considering more health states and varying the transition dynamics between them. For instance, the set of health states can comprise $Y_v(t) = R$ if v has recovered from the disease and cannot be infected again (recovered or removed state), or $Y_v(t) = H$ if v is hospitalized.

Following [40], we introduce a parameter $\rho \in [0, 1]$ to couple the network dynamics with the disease spreading. This parameter measures the activity reduction of an infected individual, such that, if $\rho = 1$, there is no activity reduction due to the disease, while, if $\rho = 0$, infected individuals cannot generate interactions. Hence, the activity of an infected node $v \in \mathcal{V}$ is reduced to a fraction ρ of its nominal activity. Formally, the activations of node $v \in \mathcal{V}$ are still governed by a Hawkes process $(N_v(t), a_v(t))$ but, if the individual is infected and becomes active, then he/she generates a connection with probability ρ, while no links are generated with probability $1 - \rho$. This probabilistic mechanism results into a split Poisson process [52].

Upon defining the health states, we should prescribe a set of mechanism to

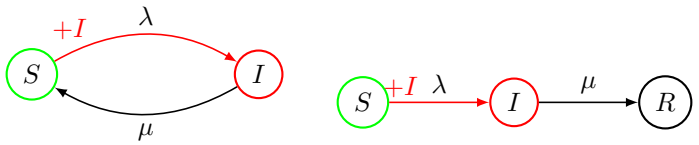

(a) SIS (b) SIR

Figure 3: State transitions characterizing the SIS and the SIR epidemic models. A susceptible node becomes infected after a contact with an infected node with probability λ. Infected nodes spontaneously recover with rate μ becoming susceptible again (SIS) or recovered (SIR).

model the possible state transitions. A possible line of approach is to hypothesize that two competing mechanisms govern the state transitions, such that

- when a link that connects a susceptible individual with an infected one is generated, the disease propagates through it with a fixed probability $\lambda \in [0, 1]$. If it propagates, then the susceptible individual also contracts the disease; and

- infected individuals spontaneously recover according to independent homogeneous Poisson processes with intensity $\mu \in \mathbb{R}_{>0}$. Recovered individuals may become susceptible again to the epidemic, in the case of the SIS model, or they become recovered and not susceptible to the epidemic, in the case of the susceptible–infected–removed (SIR) model.

The mechanisms that describe the state transitions in an SIS and in an SIR epidemic model are sketched in Fig. 3. The inclusion of more states and transition mechanisms in the epidemic model [26] allows for a closer description of the variety of real-world diseases [24], toward the implementation of accurate real-time prediction algorithms of an epidemic outbreak. In this paper, we focus on the SIS model, for which rigorous analytical results can be established. However, when possible, we present results that apply to SIR as well; for example, we illustrate our general approach to parameter identification on an SIR model. Extensions to more complex epidemic dynamics will be the subject of further studies.

Formally, the state vector $Y(t)$ evolves according to a continuous-time n-dimensional Markov process on a state space given by all the possible combinations of health states among individuals, whose size grows exponentially with n. For large-scale systems, it is possible to approximate the Markov process using a system of differential equations with arbitrary accuracy [57, 58]. In Section 5, we leverage this approximation to perform a rigorous analysis of the SIS epidemic model.

4. Parameter identification from epidemic data

Inspired by [50], we propose a technique to estimate the parameters of the self-excitement mechanisms, that is, the jump J, the forgetting rate γ, and the background activity distribution, $\hat{a}$, from epidemics data sampled at the population level. For many epidemic diseases, such as influenza, National and State health departments release weekly surveillance reports on the status of the outbreak [59]. From these reports, which include the weekly percentage of hospitalizations and outpatient visits caused by influenza-like illness, epidemiologists usually derive estimates of the evolution of the epidemic prevalence[1] in the entire population [60].

Starting from the available data, in the form of epidemic prevalence sampled weekly at the population level, we propose an algorithm to estimate the three parameters of the self-excitement mechanism. In our implementation, we assume that the disease parameters (the infection probability λ and the recovery rate μ) and the background activity distribution $\hat{a}(p)$, parametrized according to a single scalar p, are known. The algorithm applies to a generic epidemic model on ADN+HP. Depending on the characteristics of the epidemic disease, we initially choose the most suitable epidemic model, following the rationale in Section 3.2. Then, the algorithm is implemented through the following steps.

1. **Inputs.** The parametrized background activity distribution $\hat{a}(p)$, the in-

[1] The epidemic prevalence is the fraction of infected individuals in a population.

fection probability λ, the recovery rate μ, and the epidemic prevalence, which is sampled on a periodic basis for k time-periods of duration T, to obtain the vector $x(0), x(T), \ldots, x(kT)$.

2. **Initialization.** Set an initial guess for the three parameters: $J = J^*$, $\gamma = \gamma^*$, and $p = p^*$. Fix the resolution of the estimates ΔJ, $\Delta\gamma$, and Δp, and the number of simulations B.

3. **Estimation.** Given the choice of parameters $J = J^*$, $\gamma = \gamma^*$, and $p = p^*$, estimate the expected evolution of the epidemic prevalence as follows:

   i. run B simulations of the epidemic process with initial conditions given by the actual epidemic prevalence recorded by surveillance data $x(0)$, up to time kT. The output of the hth simulation is a continuous-time sample path $x_h^*(t)$, $t \in [0, kT]$;

   ii. for $i = 1, \ldots, k$, estimate the average evolution of the epidemic prevalence as

   $$x^*(iT) = \frac{1}{B} \sum_{h=1}^{B} x_h^*(iT); \qquad \text{and} \tag{9}$$

   iii. compute the estimation error

   $$E := \frac{1}{k} \sum_{i=1}^{k} |x^*(iT) - x(iT)|. \tag{10}$$

4. **Exploration.** Explore any possible variation in the parameter space that could lead to an improvement in the estimation error. Specifically,

   i. repeat the procedure in step 3. for all the six possible variation, that is, by setting $J = J^* \pm \Delta J$, $\gamma = \gamma^* \pm \Delta\gamma$, and $p = p^* \pm \Delta p$; and

   ii. for each of the three parameters $v \in \{J, \gamma, p\}$ and for each variation (increasing/decreasing), compute the corresponding estimation error $E_v^{\pm}$.

5. **Termination.** If $\min E_v^{\pm} < E$, update the parameters by choosing the values that minimize the error and the algorithm is resumed to step 3.;

otherwise, the algorithm is terminated and the output is $J = J^*$, $\gamma = \gamma^*$, and $p = p^*$.

Remark 3. *With a slightly different implementation of the algorithm, one could also estimate the disease parameters. However, since the number of variations to be explored increases linearly with the number of parameters to be estimated, an implementation in which also the disease parameters are estimated would sensibly increase the computational effort, with the risk of data overfitting. Also, disease parameters such as probability of infection and recovery rate are often estimated with a good accuracy by epidemiologists working in the field [61, 62].*

Remark 4. *The accuracy and the computational time of this algorithm are subject to the initialization of the parameters, which calls for a preliminary step where reasonable guesses about the order of magnitude of the parameters must be drawn based on numerical simulations and real-world evidence. Noise and adaptive resolutions can also be included to improve on the result, similar to standard gradient descent algorithms [63].*

To validate the algorithm and assess its performance, we test the proposed method against two synthetic datasets, generated by sampling two different realizations of the epidemic process introduced in Section 3. The first one is obtained by simulating the SIS model described in Fig. 3a with $n = 5.000$, $\lambda = 0.4$, $\mu = 0.1$, $J = 0.2$, $\gamma = 0.4$, and homogeneous background activity distribution with $a_v = 0.2$, for all the nodes. The second case is generated by sampling the SIR model described in Fig. 3b with the same population size and epidemic parameters, $J = 0.1$, $\gamma = 0.3$, and power-law distributed background activities with negative exponent -2.5 and lower cutoff at 0.1. We use the proposed algorithm to identify the model parameters. In both scenarios, we initialize $\gamma^* = 0.5$ and $J^* = 0.15$, while the homogeneous activity and the exponent of the power-law are initially set as 0.15 and -2, respectively. The resolution for each parameter is fixed at 0.005, that is, $\Delta J = \Delta\gamma = \Delta p = 0.005$.

The algorithm identifies the model parameters with high accuracy. For the SIS model, it estimates $J = 0.2$, $\gamma = 0.41$, and homogeneous background activity

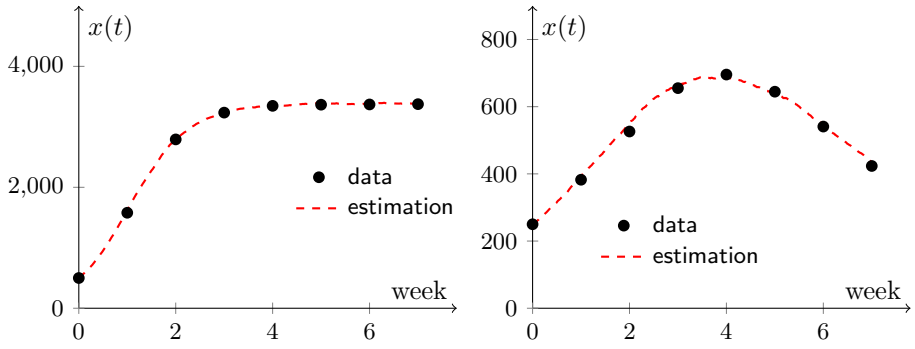

(a) SIS model (b) SIR model

Figure 4: Comparison between empirical data (black circles) and Monte Carlo estimation (over 100 independent simulations) of the evolution of the epidemic prevalence (solid curve) using the parameters estimated using the algorithm for the (a) SIS model and the (b) SIR model.

equal to $\hat{a}_v = 0.205$, against real values of $J = 0.2$, $\gamma = 0.4$, and $\hat{a}_v = 0.2$. For the SIR model, it identifies $J = 0.1$, $\gamma = 0.295$, and exponent of the power-law equal to $\alpha = -2.495$, against real values of $J = 0.1$, $\gamma = 0.3$, and $\alpha = -2.5$. In Fig. 4, we compare the Monte Carlo estimation of the evolution of the epidemic prevalence computed using the parameter identified by the model with empirical data.

Finally, we demonstrate the use of our algorithm on real-world epidemic data on the 2018–2019 seasonal influenza in Italy, available in [64]. We consider the first 10 weeks of year 2019, which embrace the peak of the seasonal outbreak [64]. Since individuals who recover from influenza are immunized, we adopt the SIR model described in Fig. 3b. To mitigate the computational effort of numerical simulations, the population size is scaled down to $n = 5,000$ units. The disease parameters are set equal to $\lambda = 0.43$ and $\mu = 0.138$, following [25]. Two different background activity distributions are tested: *i*) homogeneous (with $\hat{a}_v$ initialized at 0.13, for all the nodes), and *ii*) power-law with negative exponent -2.09, as in [65] (with the lower cutoff ε initialized at 0.08). Monte Carlo simulations are averaged over $B = 200$ simulations. In both scenarios, we

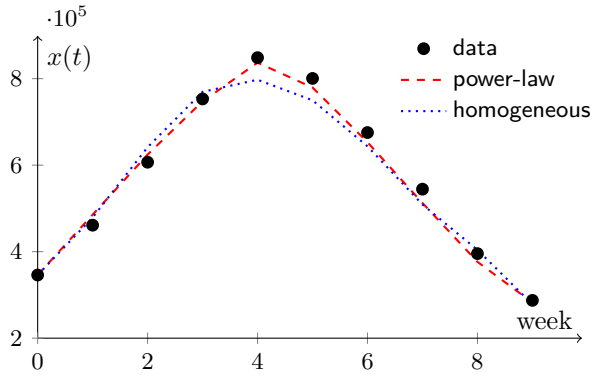

Figure 5: Monte Carlo estimation (over 100 independent simulations) of the evolution of the epidemic prevalence using homogeneous activity (blue dotted) and power-law (red dashed) with the parameters estimated in Tab. 1 compared with empirical data of 2018–2019 influenza outbreak in Italy (black circles).

	J	γ	$\hat{a}_v$	ε	average error
Homogeneous	0.12	0.285	0.135		4.51%
Power-law	0.13	0.385		0.1	3.18%

Table 1: Parameters identified for the 2018–2019 influenza outbreak in Italy.

initialize $\gamma^* = 0.2$ and $J^* = 0.05$ and the resolution for each parameter is chosen as $\Delta J = \Delta\gamma = \Delta p = 0.005$. All the initializations are based on preliminary simulations of the epidemic process. The results of our analysis are summarized in Tab. 1. From Fig. 5, one can observe that the power-law distribution yields a slightly smaller average error and better follows the peak of the epidemic outbreak, registered in the fourth week of the dataset. Following a similar procedure, one might test different distributions for the background activities and, by comparing the outputs of the algorithm, identify the distribution that best fits the observed empirical data.

5. Analytical results for the SIS model

Here, we analytically study the effect of self-excitement and activity reduction of infected individuals on the epidemic threshold of an SIS model in the

thermodynamic limit of $n \to \infty$. The SIS model, sketched in Fig. 3a, is characterized by the presence of a phase transition between a fast extinction regime and an endemic regime, which is regulated by the quantity σ called epidemic threshold [66]. Such an epidemic threshold depends on the structure of the network of interactions among individuals [67, 68]. In the thermodynamic limit, if $\lambda/\mu < \sigma$, the system is in the fast extinction regime and all the trajectories quickly converge to the disease-free equilibrium. On the contrary, if $\lambda/\mu > \sigma$, the system is in the endemic regime and trajectories with nonzero initial conditions do not reach the disease-free equilibrium, until a time exponentially long in n has elapsed [68, 69].

As noted earlier, the system evolves as a Markov process on the state space $\{I, S\}^{\mathcal{V}}$, whose size grows exponentially with the population size, thereby hindering its analysis for large-scale systems. Following [26, 70], we consider a continuous relaxation of the dynamics by studying the evolution of the probability that any individual is infected, denoted by $y_v(t) := \mathbb{P}[Y_v(t) = I]$. This probability evolves in time according to the differential equation [26, 47]

$$\frac{dy_v}{dt} = -\mu y_v + \lambda(1 - y_v)\left(a_v \frac{1}{n}\sum_{w\in\mathcal{V}} y_w + \frac{1}{n}\sum_{w\in\mathcal{V}} \rho a_w y_w\right). \tag{11}$$

From (11), one can observe that the probability that a node v is infected is controlled by three terms. The first one is negative and accounts for the spontaneous recovery process. The other two terms are both positive: the former quantifies the effect of links generated by v toward infected nodes, and the latter is the contribution of infected nodes that generate connections with v. The parameter ρ influences only this last term, due to the activity reduction in the infected state.

We compute the epidemic threshold by studying the linear stability of the disease-free equilibrium for the continuous relaxation, relying on the analytical results in [57, 58]. Therein, it has been rigorously proved that the evolution of the epidemic prevalence in the Markov process can be approximated via the continuous relaxation in (11), with exponential accuracy in the population size. Specifically, in the thermodynamic limit, the evolution of the epidemic

prevalence in the Markov process and in its counterpart in the continuous-state approximation coincide almost surely. The results of our analysis are summarized in the following theorem.

Theorem 1. *Under Assumption 1, the epidemic threshold of an SIS epidemic model on an ADN+HP with activity reduction due to infection with parameter* $\rho \in [0,1]$ *is*

$$\sigma_{HP} = \frac{1 - J/\gamma}{\frac{1+\rho}{2}\langle \hat{a} \rangle + \sqrt{\frac{(1-\rho)^2}{4}\langle \hat{a} \rangle^2 + \rho \langle \hat{a}^2 \rangle + \rho \frac{J^2}{2\gamma}\langle \hat{a} \rangle}}. \tag{12}$$

Proof The proof is based on the change of variables

$$x_i = \frac{1}{n}\sum_{v \in \mathcal{V}} a_v^{i-1} y_v, \qquad i \in \mathbb{Z}^+, \tag{13}$$

and on the stability analysis of the origin in the new set of variables. The first two variables x_1 and x_2 have a clear physical interpretation: x_1 counts the fraction of infected individuals, and x_2 measures their average activity. We notice that $x_1 = 0$ implies that: *i)* $y_v = 0$ for any $v \in \mathcal{V}$, and *ii)* $x_j = 0$ for any $j \in \mathbb{Z}^+$. Hence, to examine the stability of the origin in (11) it is sufficient to study the linear stability of $x_1 = 0$. By differentiating x_1 and using (6), (11) and (13), we establish the following differential equation:

$$\begin{aligned}
\frac{dx_1}{dt} &= \frac{1}{n}\sum_{v \in \mathcal{V}} \frac{dy_v}{dt} \\
&= \frac{1}{n}\sum_{v \in \mathcal{V}} \left[-\mu y_v + \lambda(1 - y_v)\left(a_v \frac{1}{n}\sum_{w \in \mathcal{V}} y_w + \frac{1}{n}\rho \sum_{w \in \mathcal{V}} a_w y_w \right) \right] \\
&= -\mu \frac{1}{n}\sum_{v \in \mathcal{V}} y_v + \lambda \frac{1}{n}\sum_{v \in \mathcal{V}} a_v \frac{1}{n}\sum_{w \in \mathcal{V}} y_w + \lambda\rho \frac{1}{n}\sum_{v \in \mathcal{V}} \frac{1}{n}\sum_{w \in \mathcal{V}} a_w y_w \\
&\quad -\lambda \frac{1}{n}\sum_{v \in \mathcal{V}} y_v a_v \frac{1}{n}\sum_{w \in \mathcal{V}} y_w - \lambda\rho \frac{1}{n}\sum_{v \in \mathcal{V}} y_v \frac{1}{n}\sum_{w \in \mathcal{V}} a_w y_w \\
&= -\mu x_1(t) + \lambda \langle a(t) \rangle x_1(t) + \lambda\rho x_2(t) - (1+\rho)\lambda x_1(t) x_2(t).
\end{aligned} \tag{14}$$

Since second-order terms do not influence the stability of the origin, the latter is determined by x_1, x_2, and $\langle a \rangle$.

Although almost sure convergence of $\langle a \rangle$ is ascertained by Lemma 2, the stability analysis of $x_2 = 0$ requires the study of a separate differential equation,

which is constructed similar to (14), that is,

$$\frac{dx_2}{dt} - \mu x_2(t) + \lambda\langle a^2(t)\rangle x_1(t) + \lambda\rho\langle a(t)\rangle x_2(t) - \lambda x_1(t)x_3(t) - \lambda\rho x_2(t)^2. \quad (15)$$

Through linearization about the origin, we determine that the stability of $x_2 = 0$ is affected by x_1, x_2, $\langle a\rangle$, and $\langle a^2\rangle$ (which also converges according to Lemma 2). Hence, we simplify the problem to the stability analysis of two linear differential equations in x_1 and x_2, that is,

$$\begin{cases} \dfrac{dx_1}{dt} &= (\lambda\langle a(\infty)\rangle - \mu)x_1 + \lambda\rho x_2, \\ \dfrac{dx_2}{dt} &= \langle a^2(\infty)\rangle x_1 + (\lambda\rho\langle a^2(\infty)\rangle - \mu)x_2, \end{cases} \quad (16)$$

whose Jacobian matrix is

$$D = \begin{bmatrix} -\mu + \lambda\dfrac{\langle\hat{a}\rangle}{1 - J/\lambda} & \lambda\rho \\ \lambda\left(\dfrac{\langle\hat{a}^2\rangle + \dfrac{J^2}{2\gamma}\langle\hat{a}\rangle}{(1 - J/\gamma)^2}\right) & -\mu + \lambda\rho\dfrac{\langle\hat{a}\rangle}{1 - J/\lambda} \end{bmatrix}. \quad (17)$$

The eigenvalues of D are equal to

$$-\mu + \frac{1+\rho}{2}\lambda\frac{\langle\hat{a}\rangle}{1 - J/\lambda} \pm \lambda\sqrt{\frac{(1-\rho)^2}{4}\langle\hat{a}\rangle^2 + \rho\langle\hat{a}^2\rangle + \rho\frac{J^2}{2\gamma}\langle\hat{a}\rangle}. \quad (18)$$

The largest eigenvalue is negative if and only if

$$\frac{\lambda}{\mu} < \frac{1 - J/\gamma}{\dfrac{1+\rho}{2}\langle\hat{a}\rangle + \sqrt{\dfrac{(1-\rho)^2}{4}\langle\hat{a}\rangle^2 + \rho\langle\hat{a}^2\rangle + \rho\dfrac{J^2}{2\gamma}\langle\hat{a}\rangle}}, \quad (19)$$

which provides the linear stability condition at the origin.

Remark 5. *In the absence of activity reduction, that is, for $\rho = 1$, the epidemic threshold in* (12) *reduces to the one computed in [47], namely*

$$\bar{\sigma}_{HP} = \frac{1 - J/\gamma}{\langle\hat{a}\rangle + \sqrt{\langle\hat{a}^2\rangle + \dfrac{J^2}{2\gamma}\langle\hat{a}\rangle}}. \quad (20)$$

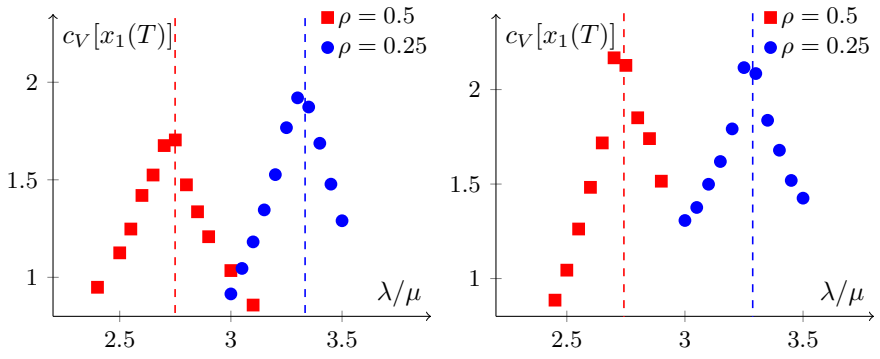

(a) Homogeneous (b) Power-law

Figure 6: Numerical estimation (over 100 independent simulations of duration $T = 100$) of the epidemic threshold for an SIS model on an ADN+HP, for different levels of activity reduction: $\rho = 0.5$ (red) and $\rho = 0.25$ (blue). The threshold is estimated by identifying the peak of the coefficient of variation $c_V[x_1(T)]$ of the fraction of infected individuals at the end of each simulation. Vertical dashed lines correspond to the analytical thresholds for the SIS model computed using Theorem 1. Common simulation parameters are $n = 2000$, $\mu = 0.138$, and initial fraction of infected nodes $x_i(0) = 0.005$, randomly selected in the population. Background activities are (a) homogeneous and (b) power-law distributed, with the parameters identified in Tab. 1.

We note that the SIR model described in Fig. 3b yields the same linearization about the origin of the SIS model in (16). Hence, in the thermodynamic limit of $n \to \infty$, the epidemic threshold of the two models coincide.

In Fig. 6, the theoretical predictions of the epidemic threshold from Theorem 1 are compared with the corresponding numerical estimation, computed using a method similar to the one proposed in [71]. Specifically, independent simulations of the dynamics are performed for a fixed time-window of duration $T = 100$, for different choices of the ratio λ/μ. For the sake of simplicity, we fix $\mu = 0.138$ (similar to [25]) and we let λ vary. Then, the threshold is estimated as the ratio λ/μ that maximizes the coefficient of variation of the fraction of infected individuals at the end of the time-window. The numerical study is performed for the two different sets of parameters identified for the case study of the 2018–2019 seasonal influenza outbreak in Italy, presented in Section 4, and for two different choices of the level of activity reduction. In all the scenarios, numerical estimations confirm the validity of theoretical predictions.

Differently from the scenario with only self-excitement in (20), where the epidemic threshold for the SIS model on an ADN+HP is always reduced, the behavior of (12) cannot be easily inferred from its expression. Depending on the relative strength of the two concurrent mechanisms, the epidemic threshold may increase or decrease, thereby unveiling a nontrivial relation between model parameters, shown in Fig. 7. In what follows, we establish a corollary that summarizes the conditions for which the epidemic threshold in Theorem 1 increases with respect to the one of a standard SIS over an ADN, where the activities of the nodes are equal to the expected asymptotic activities in the ADN+HP model.

Corollary 1. *The increase in the epidemic threshold caused by the activity reduction of infected nodes overcomes the decrease due to self-excitement if and only if*

$$\rho < 1 - \frac{J^2/\gamma}{2\dfrac{\langle \hat{a}^2 \rangle}{\langle \hat{a} \rangle} + 2\sqrt{\langle \hat{a}^2 \rangle} + \dfrac{J^2}{\gamma}}. \tag{21}$$

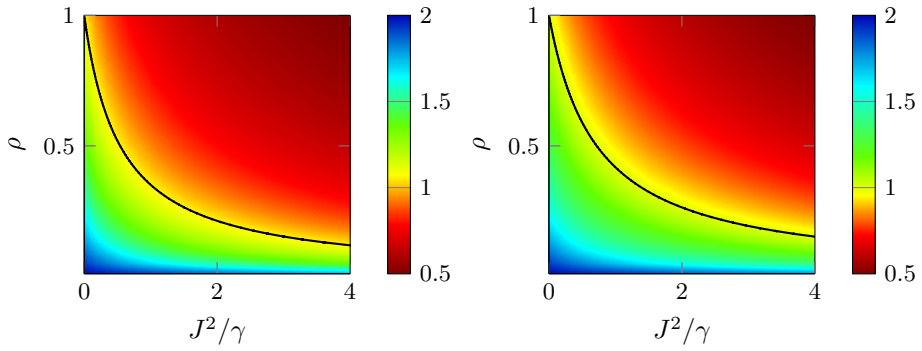

(a) Homogeneous

(b) Power-law

Figure 7: Variation of the epidemic threshold in the presence of self-excitement and activity reduction due to infection, as function of J^2/γ and ρ. The black curve from (26) separates the two regions of the parameter space where the threshold decreases (above), favoring the spread, from the one where it is increased (below). The color maps code the ratio between the epidemic threshold computed in Theorem 1 with respect to the one of a standard ADN model. The darker the red, the more the spread is favored in the ADN+HP model, the darker the blue, the more it is hindered. Background activities are (a) homogeneous and (b) power-law distributed, with the parameters identified in Tab. 1.

Proof We compare the epidemic threshold in Theorem 1, with the one of a standard SIS on an ADN [4], where the activities of the nodes are equal to the expected asymptotic activities in the ADN+HP model, that is, $\hat{a}_v/(1-J/\gamma)$, for every $v \in \mathcal{V}$ to obtain

$$\frac{\sigma_{HP}}{\sigma_{ADN}} = \frac{\langle \hat{a} \rangle + \sqrt{\langle \hat{a}^2 \rangle}}{\frac{1+\rho}{2}\langle \hat{a} \rangle + \sqrt{\frac{(1-\rho)^2}{4}\langle \hat{a} \rangle^2 + \rho \langle \hat{a}^2 \rangle + \rho \frac{J^2}{2\gamma}\langle \hat{a} \rangle}}. \tag{22}$$

By setting the ratio in (22) to be larger than 1 and moving all the square roots to the right-hand-side of the inequality, we establish

$$\frac{1-\rho}{2}\langle \hat{a} \rangle > \sqrt{\frac{(1-\rho)^2}{4}\langle \hat{a} \rangle^2 + \rho \langle \hat{a}^2 \rangle + \rho \frac{J^2}{2\gamma}\langle \hat{a} \rangle} - \sqrt{\langle \hat{a}^2 \rangle}. \tag{23}$$

By taking the square of both sides and performing some algebraic manipulations, we compute

$$(1+\rho)\langle \hat{a}^2 \rangle + \rho \frac{J^2}{2\gamma}\langle \hat{a} \rangle > \sqrt{(1-\rho)^2 \langle \hat{a} \rangle^2 \langle \hat{a}^2 \rangle + 4\rho \langle \hat{a}^2 \rangle^2 + \rho \frac{2J^2}{\gamma}\langle \hat{a} \rangle \langle \hat{a}^2 \rangle}. \tag{24}$$

By squaring again both sides to eliminate the square root and conducting a few more algebraic manipulations, we finally achieve

$$\frac{\rho}{1-\rho} > 2\frac{\gamma}{J^2}\left[\frac{\langle \hat{a}^2 \rangle}{\langle \hat{a} \rangle} + \sqrt{\langle \hat{a}^2 \rangle}\right], \tag{25}$$

which yields the claim.

Remark 6. *From the analysis of the claim in Corollary 1, one can conclude that the critical value of ρ for which the activity reduction of infected nodes overcomes the negative effect of self-excitement has a monotonic behavior with respect to the model parameters. Specifically, it increases as J and $\langle \hat{a} \rangle$ increase, and it decreases as γ and $\langle \hat{a}^2 \rangle$ increase. Hence, networks with a highly heterogeneous activity distribution require a stronger level of activity reduction to compensate for the presence of self-excitement than homogeneous networks.*

6. Enforcing activity reduction through external intervention

Although individuals should tend to spontaneously diminish their activity upon contracting the infection, such an endogenous reduction could not be suf-

ficient to bring the epidemic disease in the fast extinction regime. Toward this aim, activity reductions could be enforced by public health authorities, through awareness campaigns and restriction policies that include hospitalization and quarantine [20, 21]. Since the implementation of these control interventions is often costly for public administrations and impinge on the rights of infected individuals, predictive modeling tools are of paramount importance. Specifically, it is critical to accurately quantify the level of activity reduction that is required for reaching the fast extinction regime to reduce economic and social costs. The target level of activity reduction is computed from Theorem 1, yielding the following corollary.

Corollary 2. *An SIS epidemic model is in the fast extinction regime if and only if*

$$\rho < \rho^* = \frac{(1-J/\gamma)^2\frac{\mu^2}{\lambda^2} - (1-J/\gamma)\frac{\mu}{\lambda}\langle\hat{a}\rangle}{\langle\hat{a}^2\rangle - \langle\hat{a}\rangle^2 + \frac{J^2}{2\gamma}\langle\hat{a}\rangle + (1-J/\gamma)\frac{\mu}{\lambda}\langle\hat{a}\rangle}. \tag{26}$$

Proof This claim is obtained by setting $\lambda/\mu < \sigma_{HP}$ in (12), after some algebraic manipulations similar to those in Corollary 1.

Remark 7. *It is clear that ρ^* decreases as $\langle\hat{a}^2\rangle$ increases, but the dependence on the other parameters is less trivial. When the parameters are such that the system is in the endemic regime according to* (20) *in the absence of activity reduction, it is possible to identify a monotonic behavior by computing the partial derivatives of* (26)*. Specifically, we determine that an increase in J and λ causes a decrease of ρ^*, whereas an increase in γ, μ, and $\langle\hat{a}\rangle$ has the opposite effect. Once the other parameters are blocked, epidemics in highly heterogeneous networks require a greater effort to be controlled.*

The prediction formalized in Corollary 2 could be utilized by practitioners to ascertain how much the activity of infected individuals should be reduced to attain fast eradication of the outbreak. To demonstrate the use of this corollary, we consider once again the case study of the 2018–2019 seasonal influenza outbreak in Italy, presented in Section 4. From Corollary 2, we establish that the

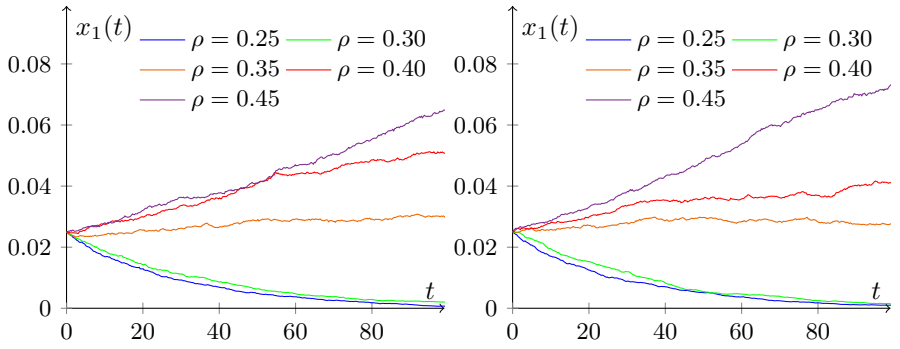

(a) Homogeneous (b) Power-law

Figure 8: Estimated evolution of the epidemic prevalence for an influenza-like SIS model on ADN+HP with different levels of activity reduction of the infected nodes. Background activities are (*a*) homogeneous and (*b*) power-law distributed, with the parameters identified in Tab. 1.

system is in the fast extinction regime if $\rho^* = 0.3313$ (under the homogeneous background distribution assumption) or $\rho^* = 0.3334$ (under the power-law assumption). Comparing these two results, predictions suggest that the desirable level of activity reduction ρ^* is robust with respect to the choice of the background activity distribution made in the parameter identification algorithm.

Figure 8 compares the evolution of the epidemic prevalence of an SIS model (averaged over 200 Monte Carlo simulations) for different choices of the activity reduction parameter ρ. The numerical simulations validate our analytical results, whereby if $\rho > \rho^*$, the disease spreads in the population (orange, red, and violet curves), while, if $\rho < \rho^*$, it is quickly eradicated (blue and green curves). By comparing the blue and the green curves (both with $\rho < \rho^*$), one observes that, once ρ is sufficiently small to reach the fast extinction regime, there is not a clear advantage of imposing further reductions, since no significant improvement can be appreciated. In this sense, Corollary 2 establishes the optimal level of activity reduction that is needed to achieve fast extinction of the disease: a higher level of activity may beget an unsuccessful effort by the public administration, which would not be sufficient to stop the epidemic outbreak; while, a

lower level of activity may lead to unnecessary costs for the administration and needless discomfort for the population, without improvements in the eradication of the disease.

7. Conclusion

Through the lens of activity driven networks, we have established a modeling framework for the analysis and control of epidemics on temporal networks that includes self-excitement mechanisms and activity reduction of infected individuals. The modeling framework is grounded in the theory of Hawkes processes, which provide a potent tool to study burstiness and temporal clustering without losing the Markov property that is needed for analytical treatment and without introducing an excessively large number of parameters. To support the application of the framework in the study of real-world data, a parameter identification technique has been proposed and validated. This algorithm takes as input data at the population level, such as the National epidemic prevalence, and outputs the parameters of the underlying Hawkes processes. The viability of the identification procedure has been demonstrated on a real-world case study of 2018–2019 seasonal influenza in Italy.

Within this framework, the susceptible–infected–susceptible epidemic model has been studied, unveiling a nontrivial interaction between self-excitement and activity reduction. If self-excitement overcomes the activity reduction, then the spread of the disease is favored and the network is more prone to the inception of an epidemic outbreak. In the opposite scenario, the system is more robust to the spread of the epidemics. Through a linear stability analysis, we have successfully characterized these two regimes, as a function of the model parameters. Based on these theoretical claims, we have addressed the epidemiological problem of estimating the level of activity reduction that is required to increase the epidemic threshold so that a fast eradication of the epidemic outbreak is observed. From a practical point of view, reducing individual activity is at the basis of standard interventions, including awareness campaigns, quarantine, and hospitalization.

The inclusion of real-world phenomena within analytically tractable epidemic models constitutes a key methodological step toward the development of accurate and reliable techniques to predict and control epidemic outbreaks. Encouraged by the results in the paper, our future research will seek to deepen the design of control strategies based on activity reduction of infected nodes. In particular, we aim at including additional real-world constraints, such as the limited amount of hospital beds that hinders the implementation of large-scale hospitalization and budget constraints for awareness campaigns. Addressing these constraints will call for fundamental research at the interface of network theory and optimization to solve control problems in stochastic, time-varying settings. We believe that the possibility to rigorously analyze the joint effect of self-excitement mechanisms and (possibly exogenous) activity reduction could find applications in spreading processes of different nature, including fake news, computer viruses, and diffusion of information.

The results of this paper contribute to an improved understanding of the interplay between two inherent characteristics of epidemics in complex social networks: burstiness due to the presence of self-excitement mechanisms and (spontaneous or enforced) activity reduction of infected nodes. Future efforts should be placed toward the extension of these claims and techniques to more complex temporal networks, encapsulating other inherent properties of social networks, such as the presence of community structures [29, 30], recurrent connections [31, 32], high-order relationships [33], and time-delays [72]. We believe that this direction of research, along the development of realistic and analytically tractable models, is necessary to unveil and understand the interplay between the critical dynamic phenomena that govern the spread of epidemic diseases in complex networks and, possibly, to leverage this knowledge toward the control of their evolution.

Acknowledgment

This work was partially supported by the National Science Foundation [grant number CMMI-1561134]; the Compagnia di San Paolo; the Italian Ministry of Education, Universities and Research [grant number E11G18000350001]; and the Italian Ministry of Foreign Affairs and International Cooperation [grant "Mac2Mic"].

References

References

[1] E. Volz, L. A. Meyers, Epidemic thresholds in dynamic contact networks, J. Royal Soc. Interface 6 (2009) 233–241. doi:10.1098/rsif.2008.0218.

[2] P. Holme, J. Saramäki, Temporal networks, Phys. Rep. 519 (2012) 97–125. doi:10.1016/j.physrep.2012.03.001.

[3] P. Holme, Modern temporal network theory: a colloquium, Eur. Phys. J. B 88 (2015) 234. doi:10.1140/epjb/e2015-60657-4.

[4] N. Perra, B. Gonçalves, R. Pastor-Satorras, A. Vespignani, Activity driven modeling of time varying networks, Sci. Rep. 2 (2012) 469. doi:10.1038/srep00469.

[5] C. T. Butts, Revisiting the foundations of network analysis, Science 325 (2009) 414–416. doi:10.1126/science.1171022.

[6] R. Pastor-Satorras, C. Castellano, P. Van Mieghem, A. Vespignani, Epidemic processes in complex networks, Rev. Mod. Phys. 87 (2015) 925–979. doi:10.1103/RevModPhys.87.925.

[7] A. Baronchelli, R. Pastor-Satorras, Mean-field diffusive dynamics on weighted networks, Phys. Rev. E 82 (2010) 011111. doi:10.1103/PhysRevE.82.011111.

[8] R. A. S. Alves, R. M. Assuncao, P. O. S. Vaz de Melo, Burstiness scale: a parsimonious model for characterizing random series of events, in: Proc. 22nd ACM SIGKDD Int. Conf. Knowledge Discovery and Data Mining, 2016, pp. 1405–1414. doi:10.1145/2939672.2939852.

[9] A.-L. Barabási, The origin of bursts and heavy tails in human dynamics, Nature 435 (2005) 207–211. doi:10.1038/nature03459.

[10] K.-I. Goh, A.-L. Barabási, Burstiness and memory in complex systems, EPL 81 (2008) 48002. doi:10.1209/0295-5075/81/48002.

[11] D. X. Horváth, J. Kertész, Spreading dynamics on networks: the role of burstiness, topology and non-stationarity, New J. Phys. 16 (2014) 073037. doi:10.1088/1367-2630/16/7/073037.

[12] R. Lambiotte, L. Tabourier, J.-C. Delvenne, Burstiness and spreading on temporal networks, Eur. Phys. J. B 86 (2013) 320. doi:10.1140/epjb/e2013-40456-9.

[13] E. W. Fox, M. B. Short, F. P. Schoenberg, K. D. Coronges, A. L. Bertozzi, Modeling e-mail networks and inferring leadership using self-exciting point processes, J. Am. Stat. Assoc. 111 (2016) 564–584. doi:10.1080/01621459.2015.1135802.

[14] R. D. Malmgren, D. B. Stouffer, A. E. Motter, L. A. N. Amaral, A poissonian explanation for heavy tails in e-mail communication, Proc. Natl. Acad. Sci. USA 105 (2008) 18153–18158. doi:10.1073/pnas.0800332105.

[15] N. Masuda, T. Takaguchi, N. Sato, K. Yano, Self-exciting point process modeling of conversation event sequences, in: Temporal Networks, 2013, pp. 245–264. doi:10.1007/978-3-642-36461-7_12.

[16] G. O. Mohler, M. B. Short, P. J. Brantingham, F. P. Schoenberg, G. E. Tita, Self-exciting point process modeling of crime, J. Am. Stat. Assoc. 106 (2011) 100–108. doi:10.1198/jasa.2011.ap09546.

[17] Q. Zhao, M. A. Erdogdu, H. Y. He, A. Rajaraman, J. Leskovec, SEISMIC: a self-exciting point process model for predicting tweet popularity, in: Proc. 21st ACM SIGKDD Int. Conf. Knowledge Discovery and Data Mining, 2015, pp. 1513–1522. doi:10.1145/2783258.2783401.

[18] S. Riley, C. Fraser, C. A. Donnelly, A. C. Ghani, L. J. Abu-Raddad, A. J. Hedley, G. M. Leung, L. M. Ho, T. H. Lam, T. Q. Thach, et al., Transmission dynamics of the etiological agent of SARS in Hong Kong: impact of public health interventions, Science 300 (2003) 1961–1966. doi:10.1126/science.1086478.

[19] M. Cotten, S. J. Watson, A. I. Zumla, Spread, circulation, and evolution of the Middle East respiratory syndrome coronavirus, MBio 5 (2014) e01062–13. doi:10.1128/mBio.01062-13.

[20] H. Hethcote, M. Zhien, L. Shengbing, Effects of quarantine in six endemic models for infectious diseases, Math. Biosci. 180 (2002) 141–160. doi:10.1016/S0025-5564(02)00111-6.

[21] M. Litvinova, Q.-H. Liu, E. S. Kulikov, M. Ajelli, Reactive school closure weakens the network of social interactions and reduces the spread of influenza, Proc. Natl. Acad. Sci. USA 116 (27) (2019) 13174–13181. doi:10.1073/pnas.1821298116.

[22] M. Karsai, N. Perra, A. Vespignani, Time varying networks and the weakness of strong ties, Sci. Rep. 4 (2014) 4001. doi:10.1038/srep04001.

[23] S. Liu, N. Perra, M. Karsai, A. Vespignani, Controlling contagion processes in activity driven networks, Phys. Rev. Lett. 112 (2014) 118702. doi:10.1103/PhysRevLett.112.118702.

[24] A. Rizzo, B. Pedalino, M. Porfiri, A network model for Ebola spreading, J. Theor. Biol. 394 (2016) 212–222. doi:10.1016/j.jtbi.2016.01.015.

[25] L. Zino, A. Rizzo, M. Porfiri, Continuous-time discrete-distribution theory for activity-driven networks, Phys. Rev. Lett. 117 (2016) 228302. doi:10.1103/PhysRevLett.117.228302.

[26] L. Zino, A. Rizzo, M. Porfiri, An analytical framework for the study of epidemic models on activity driven networks, J. Complex Netw. 5 (2017) 924–952. doi:10.1093/comnet/cnx056.

[27] I. Pozzana, K. Sun, N. Perra, Epidemic spreading on activity-driven networks with attractiveness, Phys. Rev. E 96 (2017) 042310. doi:10.1103/PhysRevE.96.042310.

[28] L. Alessandretti, K. Sun, A. Baronchelli, N. Perra, Random walks on activity-driven networks with attractiveness, Phys. Rev. E 95 (2017) 052318. doi:10.1103/PhysRevE.95.052318.

[29] M. Nadini, K. Sun, E. Ubaldi, M. Starnini, A. Rizzo, N. Perra, Epidemic spreading in modular time-varying networks, Sci. Rep. (2018) 2352doi:10.1038/s41598-018-20908-x.

[30] C. Bongiorno, L. Zino, A. Rizzo, A novel framework for community modeling and characterization in directed temporal networks, Appl. Netw. Sci. 4 (2019) 10. doi:10.1007/s41109-019-0119-2.

[31] Y. Lei, X. Jiang, Q. Guo, Y. Ma, M. Li, Z. Zheng, Contagion processes on the static and activity-driven coupling networks, Phys. Rev. E 93 (2016) 032308. doi:10.1103/PhysRevE.93.032308.

[32] M. Nadini, A. Rizzo, M. Porfiri, Epidemic spreading in temporal and adaptive networks with static backbone, IEEE Trans. Netw. Sci. Eng. *Published online*. doi:10.1109/TNSE.2018.2885483.

[33] G. Petri, A. Barrat, Simplicial activity driven model, Phys. Rev. Lett. 121 (2018) 228301. doi:10.1103/PhysRevLett.121.228301.

[34] D. Li, D. Han, J. Ma, M. Sun, L. Tian, T. Khouw, H. E. Stanley, Opinion dynamics in activity-driven networks, EPL 120 (2017) 28002. doi:10.1209/0295-5075/120/28002.

[35] A. Rizzo, M. Porfiri, Innovation diffusion on time-varying activity driven networks, Eur. Phys. J. B 89 (2016) 20. doi:10.1140/epjb/e2015-60933-3.

[36] H. Zhu, J. Ma, S. Li, Effects of online and offline interaction on rumor propagation in activity-driven networks, Physica A 525 (2019) 1124–1135. doi:https://doi.org/10.1016/j.physa.2019.04.006.

[37] M. Starnini, R. Pastor-Satorras, Temporal percolation in activity-driven networks, Phys. Rev. E 89 (2014) 032807. doi:10.1103/PhysRevE.89.032807.

[38] K. Sun, A. Baronchelli, N. Perra, Contrasting effects of strong ties on SIR and SIS processes in temporal networks, Eur. Phys. J. B 88 (2015) 326. doi:10.1140/epjb/e2015-60568-4.

[39] M. Tizzani, S. Lenti, E. Ubaldi, A. Vezzani, C. Castellano, R. Burioni, Epidemic spreading and aging in temporal networks with memory, Phys. Rev. E 98 (2018) 062315. doi:10.1103/PhysRevE.98.062315.

[40] A. Rizzo, M. Frasca, M. Porfiri, Effect of individual behavior on epidemic spreading in activity driven networks, Phys. Rev. E 90 (2014) 042801. doi:10.1103/PhysRevE.90.042801.

[41] A. Moinet, R. Pastor-Satorras, A. Barrat, Effect of risk perception on epidemic spreading in temporal networks, Phys. Rev. E 97 (2018) 012313. doi:10.1103/PhysRevE.97.012313.

[42] E. Ubaldi, A. Vezzani, M. Karsai, N. Perra, R. Burioni, Burstiness and tie activation strategies in time-varying social networks, Sci. Rep. 7 (2017) 46225. doi:10.1038/srep46225.

[43] M. Mancastroppa, A. Vezzani, M. A. Muñoz, R. Burioni, Burstiness in activity-driven networks and the epidemic threshold, J. Stat. Mech.: Theory Exp. 2019 (2019) 053502. doi:10.1088/1742-5468/ab16c4.

[44] A. G. Hawkes, Spectra of some self-exciting and mutually exciting point processes, Biometrika 58 (1971) 83–90. doi:10.1093/biomet/58.1.83.

[45] D. Marsan, O. Lengliné, Extending earthquakes' reach through cascading, Science 319 (2008) 1076–1079. doi:10.1126/science.1148783.

[46] D. T. Gillespie, A general method for numerically simulating the stochastic time evolution of coupled chemical reactions, J. Comput. Phys. 22 (1976) 403–434. doi:10.1016/0021-9991(76)90041-3.

[47] L. Zino, A. Rizzo, M. Porfiri, Modeling memory effects in activity-driven networks, SIAM J. Appl. Dyn. Syst. 17 (2018) 2830–2854. doi:10.1137/18M1171485.

[48] J. Rasmussen, Bayesian inference for hawkes processes, Methodol. Comput. Appl. Probab. 15 (3) (2013) 623–642. doi:10.1007/s11009-011-9272-5.

[49] J. Da Fonseca, R. Zaatour, Hawkes process: fast calibration, application to trade clustering, and diffusive limit, J. Futures Mark. 34 (2014) 548–579. doi:10.1002/fut.21644.

[50] L. Kim, M. Abramson, K. Drakopoulos, S. Kolitz, A. Ozdaglar, Estimating social network structure and propagation dynamics for an infectious disease, in: Social Computing, Behavioral-Cultural Modeling and Prediction, 2014, pp. 85–93. doi:10.1007/978-3-319-05579-4_11.

[51] L. Zino, A. Rizzo, M. Porfiri, Effect of self-excitement and behavioral factors on epidemics on activity driven networks, in: Proc. 18th Europ. Control Conf., 2019, pp. 1512–1517. doi:10.23919/ECC.2019.8795748.

[52] N. T. J. Bailey, The Elements of Stochastic Processes with Applications to the Natural Sciences, 1st Edition, John Wiley & Sons, New York NY, USA, 1990.

[53] B. Øksendal, Stochastic Differential Equations: An Introduction with Applications, 6th Edition, Springer, Berlin, Germany, 2003. doi:10.1007/978-3-642-14394-6.

[54] A. Dassios, H. Zhao, Exact simulation of Hawkes process with exponentially decaying intensity, Electron. Commun. Probab. 18 (2013) 62–74. doi:10.1214/ECP.v18-2717.

[55] T. Hoffmann, M. A. Porter, R. Lambiotte, Generalized master equations for non-poisson dynamics on networks, Phys. Rev. E 86 (2012) 046102. doi:10.1103/PhysRevE.86.046102.

[56] M. Kivelä, M. A. Porter, Estimating interevent time distributions from finite observation periods in communication networks, Phys. Rev. E 92 (2015) 052813. doi:10.1103/PhysRevE.92.052813.

[57] T. G. Kurtz, Solutions of ordinary differential equations as limits of pure jump Markov processes, J. Appl. Probab. 7 (1970) 49–58. doi:10.2307/3212147.

[58] T. G. Kurtz, Limit theorems for sequences of jump Markov processes approximating ordinary differential processes, J. Appl. Probab. 8 (1971) 344–356. doi:10.2307/3211904.

[59] CDC Centers for Disease Control and Prevention, Weekly U.S. Influenza Surveillance Report, accessed on October 23, 2019.
URL https://www.cdc.gov/flu/weekly/

[60] C. Reed, S. S. Chaves, P. Daily Kirley, R. Emerson, D. Aragon, E. B. Hancock, L. Butler, J. Baumbach, G. Hollick, N. M. Bennett, M. R. Laidler, A. Thomas, M. I. Meltzer, L. Finelli, Estimating influenza disease burden from population-based surveillance data in the united states, PLoS ONE 10 (2015) 1–13. doi:10.1371/journal.pone.0118369.

[61] V. Clamer, I. Dorigatti, L. Fumanelli, C. Rizzo, A. Pugliese, Estimating transmission probability in schools for the 2009 H1N1 influenza pan-

demic in Italy, Theor. Biol. Med. Model. 13 (2016) 19. doi:10.1186/s12976-016-0045-2.

[62] T.-C. Chan, T.-H. Hu, J.-S. Hwang, Estimating the risk of influenza-like illness transmission through social contacts: Web-based participatory cohort study, JMIR Public Health Surveill. 4 (2018) e40. doi:10.2196/publichealth.8874.

[63] S. Ruder, An overview of gradient descent optimization algorithms, arXiv preprint.
URL http://arxiv.org/abs/1609.04747

[64] Istituto Superiore di Sanità (National Institute of Health), Sistema di Sorveglianza Integrata dell'Influenza (in Italian), accessed on October 23, 2019.
URL https://old.iss.it/site/RMI/influnet/pagine/rapportoInflunet.aspx

[65] W. Aiello, F. Chung, L. Lu, A random graph model for massive graphs, in: Proc. 32nd Ann. ACM Symp. Theory of Computing, 2000, pp. 171–180. doi:10.1145/335305.335326.

[66] N. T. J. Bailey, The Mathematical Theory of Infectious Diseases and its Applications, 2nd Edition, Griffin, London, UK, 1975.

[67] R. Pastor-Satorras, A. Vespignani, Epidemic spreading in scale-free networks, Phys. Rev. Lett. 86 (2001) 3200. doi:10.1103/PhysRevLett.86.3200.

[68] A. Ganesh, L. Massoulié, D. Towsley, The effect of network topology on the spread of epidemics, in: Proc. IEEE INFOCOM, Vol. 2, 2005, pp. 1455–1466.

[69] F. Fagnani, L. Zino, Diffusion of innovation in large scale graphs, IEEE Trans. Netw. Sci. Eng. 4 (2017) 100–111. doi:10.1109/TNSE.2017.2678202.

[70] P. Van Mieghem, J. Omic, R. Kooij, Virus spread in networks, IEEE/ACM Trans. Netw. 17 (2009) 1–14. doi:10.1109/TNET.2008.925623.

[71] S. C. Ferreira, C. Castellano, R. Pastor-Satorras, Epidemic thresholds of the susceptible-infected-susceptible model on networks: A comparison of numerical and theoretical results, Phys. Rev. E 86 (2012) 041125. doi:10.1103/PhysRevE.86.041125.

[72] Q. Li, B. Shen, Z. Wang, T. Huang, J. Luo, Synchronization control for a class of discrete time-delay complex dynamical networks: A dynamic event-triggered approach, IEEE Trans. Cybern. 49 (2019) 1979–1986. doi:10.1109/TCYB.2018.2818941.